

Effects of Single-site Anisotropy on Mixed Diamond Chains with Spins 1 and 1/2

Kazuo HIDA* and Ken'ichi TAKANO¹

*Division of Material Science, Graduate School of Science and Engineering,
Saitama University, Saitama, Saitama, 338-8570*

¹*Toyota Technological Institute, Tenpaku-ku, Nagoya 468-851*

(Received June 20, 2011)

Effects of single-site anisotropy on mixed diamond chains with spins 1 and 1/2 are investigated in the ground states and at finite temperatures. There are phases where the ground state is a spin cluster solid, i.e., an array of uncorrelated spin-1 clusters separated by singlet dimers. The ground state is nonmagnetic for the easy-plane anisotropy, while it is paramagnetic for the easy-axis anisotropy. Also, there are the Néel, Haldane, and large- D phases, where the ground state is a single spin cluster of infinite size and the system is equivalent to the spin-1 Heisenberg chain with alternating anisotropy. The longitudinal and transverse susceptibilities and entropy are calculated at finite temperatures in the spin-cluster-solid phases. Their low-temperature behaviors are sensitive to anisotropy.

KEYWORDS: mixed diamond chain, anisotropy, frustration, spin cluster solid, Néel phase, Haldane phase, large- D phase

1. Introduction

Frustration in quantum spin systems has been one of the most exciting subjects studied in the field of magnetism over these past decades.^{1,2)} A number of theoretical and experimental investigations have revealed exotic phenomena induced by the interplay of frustration and quantum fluctuation. In the theoretical approach, many exactly solvable models have played crucial roles in elucidating frustrated quantum magnetism. As typical examples, there exists a class of models whose ground states are exact spin cluster solid (SCS) states because of frustration. The SCS state is defined as a tensor product state of exact local eigenstates of cluster spins. A dimer state is the simplest type of SCS state. For example, the Majumdar-Ghosh model³⁾ has a dimer ground state, which is a prototype of spontaneously dimerized states in one-dimensional frustrated magnets.⁴⁾ The Shastry-Sutherland model,⁵⁾ which corresponds to the material $\text{SrCu}_2(\text{BO}_3)_2$,^{6,7)} also has a dimer ground state.

The diamond chain is a frustrated spin chain with exact SCS ground states that are different from dimer states. The lattice structure of the diamond chain is shown in Fig. 1. In a unit cell, there are two kinds of nonequivalent lattice sites occupied by spins with magnitudes S and τ ; we denote the set of magnitudes by (S, τ) . One of the authors and coworkers^{8,9)} introduced this lattice structure and generally investigated the case of (S, S) , i.e., the pure diamond chain (PDC). After that, Niggemann et al.^{10,11)} argued about a series of diamond chains with $(S, 1/2)$.

The mixed diamond chain (MDC) is defined as a diamond chain with $(S, S/2)$ for the integer S .¹²⁾ Recently, extensive investigation on the MDC has been carried out by the present authors.¹²⁻¹⁵⁾ The MDC is of special interest among diamond chains, because only the MDC has the Haldane phase in the absence of frustration so that we can observe the transition from the Haldane phase

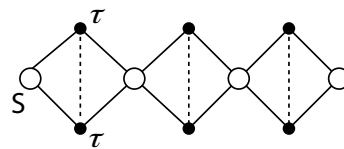


Fig. 1. Structure of the diamond chain. Spin magnitudes in a unit cell are indicated by S and τ ; we denote the set of magnitudes by (S, τ) . The PDC is the case of $S = \tau$, while the MDC is the case of $S = 2\tau$ with integer or half-odd integer τ .

to a SCS phase induced by frustration. In contrast, diamond chains of other types have ferrimagnetic ground states for weak frustration.

The common features of any types of diamond chains are that they have an infinite number of local conservation laws and more than two different types of exact SCS ground states are realized depending on the strength of frustration. The MDC with $(1, 1/2)$ has 3 different paramagnetic SCS phases accompanied by spontaneous translational symmetry breakdown (STSB) and one paramagnetic phase without STSB in addition to a nonmagnetic Haldane ground state in a less frustrated region.^{10,12)} The SCS structures of the ground states are also reflected in characteristic thermal properties, as reported in ref. 13.

Thus, the diamond chain serves as a playground for investigating various additional effects on frustrated magnetism on a well-founded basis. Therefore, various modifications of the PDC and MDC have been examined by many researchers.¹⁴⁻¹⁹⁾ It is found that the natural mineral azurite consists of distorted PDCs with spin 1/2 and the magnetic properties of this material have been experimentally studied in detail.^{20,21)} Other materials have also been reported.^{22,23)} In addition, as reviewed in ref. 14, the MDC is related to many other important models of frustrated magnetism.²⁴⁻³³⁾

In the present work, we concentrate on the effects

*E-mail address: hida@mail.saitama-u.ac.jp

of the single-site anisotropy D on the ground-state and finite-temperature properties of the MDC with $(1,1/2)$. In many quantum spin systems, it is known that the D -term changes the ground state drastically. A well-known example is the effect of the D -term on the Haldane state of spin-1 antiferromagnetic Heisenberg chains. A large positive D term destroys the hidden order in the Haldane phase and drives the ground state into the large- D phase that has no specific order. On the other hand, a large negative D -term stabilizes the Néel order.^{34–39)} The D -terms in the higher spin and mixed spin Heisenberg chains induce rich phase diagrams.^{39–42)} The alternating D -terms in spin-1 Heisenberg chains can pin the fluctuating hidden order to induce a long-period Néel order.⁴³⁾ They can also induce the partial ferrimagnetic order in higher-spin chains.⁴⁴⁾ Considering the high degeneracy of the ground states of the MDC,¹²⁾ we may expect an even richer phase diagram in the MDC with the single-site anisotropy.

Thus far, despite the theoretical relevance of the MDC, no materials described by the MDC have been found. Nevertheless, synthesizing MDC materials is not an unrealistic expectation in view of the successful synthesis of many novel magnetic materials such as molecule-based magnetic materials.⁴⁵⁾ In general, it is natural to expect the single-site anisotropy on the spin-1 site in real MDC compounds. From this viewpoint, it is important to present theoretical predictions on the ground state and finite-temperature properties of anisotropic MDCs to widen the range of candidate materials of the MDC and raise the possibility of their synthesis. We find that the effect of the single-site anisotropy not only gives quantitative correction to physical quantities but also changes the ground state and low-temperature behavior qualitatively. Among them, the SCS ground states are found to be sensitive to such anisotropy.

This paper is organized as follows. In §2, the Hamiltonian for the MDC with the single-site anisotropy is presented. In §3, the MDC with the single-site anisotropy is examined by numerical methods and the ground-state phase diagram is obtained. Various limiting cases in the phase diagram are discussed by the perturbation method. In §4, the finite-temperature behaviors of the longitudinal and transverse susceptibilities and entropy are investigated numerically and analytically by extending the method developed in ref. 13. The last section is devoted to the summary and discussion.

2. Hamiltonian

We consider the MDC with the single-site anisotropy on spin-1 sites described by the Hamiltonian

$$\mathcal{H} = J \sum_{l=1}^L \left[(\mathbf{S}_l + \mathbf{S}_{l+1}) \cdot (\boldsymbol{\tau}_l^{(1)} + \boldsymbol{\tau}_l^{(2)}) + \lambda \boldsymbol{\tau}_l^{(1)} \boldsymbol{\tau}_l^{(2)} \right] + D \sum_{l=1}^L S_l^z{}^2, \quad (1)$$

where \mathbf{S}_l is the spin-1 operator, and $\boldsymbol{\tau}_l^{(1)}$ and $\boldsymbol{\tau}_l^{(2)}$ are the spin-1/2 operators in the l th unit cell. The total number of unit cells is denoted by L . In the case of $D = 0$, eq. (1)

reduces to the Hamiltonian of the isotropic MDC.¹²⁾ In what follows, we set the energy unit as $J = 1$.

Before proceeding, we analyze the classical version of the quantum Hamiltonian (1). We obtain the classical ground state for any λ and D in Appendix. We have four classical phases separated by the phase boundaries $\lambda = 2$ and $D = 0$. In the two phases of $\lambda > 2$, the ground-state spin configurations can be locally modified without an energy increase. This classical situation corresponds to the quantum situation that there are an infinite number of low-energy states that are transformed from each other by local modification. Such quasi-degenerate low-energy states may enhance quantum fluctuations to contribute to the appearance of exotic quantum states for large λ in the quantum system even for finite D .

3. Ground-State Phase Diagram

3.1 General formulation for phase boundaries

The Hamiltonian (1) has a series of conservation laws. To see it, we rewrite eq. (1) in the form

$$\mathcal{H} = \sum_{l=1}^L \left[(\mathbf{S}_l \mathbf{T}_l + \mathbf{T}_l \mathbf{S}_{l+1}) + \frac{\lambda}{2} \left(\mathbf{T}_l^2 - \frac{3}{2} \right) \right] + D \sum_{l=1}^L S_l^z{}^2, \quad (2)$$

where the composite spin operators \mathbf{T}_l are defined as

$$\mathbf{T}_l \equiv \boldsymbol{\tau}_l^{(1)} + \boldsymbol{\tau}_l^{(2)} \quad (l = 1, 2, \dots, L). \quad (3)$$

Then, it is evident that

$$[\mathbf{T}_l^2, \mathcal{H}] = 0 \quad (l = 1, 2, \dots, L). \quad (4)$$

Thus, we have L conserved quantities \mathbf{T}_l^2 for all l , even for $D \neq 0$. By defining the magnitude T_l of \mathbf{T}_l by $\mathbf{T}_l^2 = T_l(T_l + 1)$, we have a set of good quantum numbers $\{T_l; l = 1, 2, \dots, L\}$. Each T_l takes a value of 0 or 1. The total Hilbert space of the Hamiltonian (2) consists of separate subspaces, each of which is specified by a definite set of $\{T_l\}$, i.e., a sequence of 0 and 1.

A spin pair of $T_l = 0$ is a singlet dimer, that cuts off the correlation between \mathbf{S}_l 's at both sides as seen from eq. (2). Hence, when a segment is bounded by two $T_l = 0$ pairs, it is isolated from other parts of the spin chain. The segment including n successive \mathbf{T}_l 's with $T_l = 1$ and $n + 1$ \mathbf{S}_l 's is called a cluster- n as in the isotropic case.¹²⁾ A cluster- n is equivalent to an antiferromagnetic Heisenberg chain consisting of $2n + 1$ effective spins with magnitude 1 with alternating anisotropy. The Hamiltonian is written as

$$\mathcal{H}_n = \sum_{l=1}^{2n} \tilde{\mathbf{S}}_l \tilde{\mathbf{S}}_{l+1} + D \sum_{l=1}^{n+1} \tilde{S}_{2l-1}^z{}^2, \quad (5)$$

where $\tilde{\mathbf{S}}_{2l-1} = \mathbf{S}_l$ and $\tilde{\mathbf{S}}_{2l} = \mathbf{T}_l$.

The ground state of the total diamond chain is analyzed by describing each cluster by the Heisenberg model (5). For $D = 0$, we have obtained the complete ground-state phase diagram in ref. 12. In particular, we found successive phase transitions between dimer-cluster- n (DC n) phases with $n = 0, 1, 2, 3$, and ∞ as λ decreases. The DC0 phase is also called the dimer monomer phase where $T_l = 0$ for all l . The DC n phase

with $n = 1, 2$, or 3 is the phase where the ground state consists of an alternating array of cluster- n 's and singlet dimers. The $\text{DC}\infty$ phase is the Haldane phase for the equivalent Heisenberg chain with $T_l = 1$ for all l . The description in terms of cluster- n and $\text{DC}n$ states is naturally extended to the finite- D regimes. By the same argument as that in ref. 12, the phase boundary between the $\text{DC}(n-1)$ and $\text{DC}n$ phases for finite D is given by

$$\begin{aligned} \lambda_c(n-1, n; D) \\ = (n+1)\tilde{E}_G(2n-1, D) - n\tilde{E}_G(2n+1, D), \end{aligned} \quad (6)$$

where $\tilde{E}_G(2n+1, D)$ is the ground-state energy of the Hamiltonian (5). These phase transitions are of the first order, since they take place as level crossings between two eigenstates of the original Hamiltonian (1) characterized by different sets of quantum numbers $\{T_l\}$. The direct transition from the $\text{DC}n$ phase to the $\text{DC}\infty$ phase takes place at

$$\lambda_c(n, \infty; D) = \tilde{E}_G(2n+1, D) - 2(n+1)\tilde{e}_G(\infty, D), \quad (7)$$

if $\lambda_c(n, \infty; D) > \lambda_c(n, n+1; D)$, where $\tilde{e}_G(\infty, D)$ is the ground-state energy of the Hamiltonian (5) with $n \rightarrow \infty$ per unit cell.

The above arguments are almost parallel to those in the isotropic case. For the physical conclusion, however, we observe a significant difference from the isotropic case, as described in the following sections.

3.2 Ground-state phase diagram determined by numerical method

To obtain the ground-state phase diagram using eqs. (6) and (7), we have numerically diagonalized the Hamiltonian (5) to calculate the ground-state energy $\tilde{E}_G(2n+1, D)$. The ground-state energy per unit cell $\tilde{e}_G(\infty, D)$ is calculated by the infinite-size DMRG by estimating the energy increment accompanied by an addition of a unit cell at the center of the chain. The phase diagram is shown in Fig. 2. Because of the presence of fine structures of the phase diagram, we present a series of phase diagrams magnified appropriately. In the top figure, the broken and dotted lines are the results of the perturbation analysis described in the next section.

The main features characteristic of the anisotropic case are as follows.

- (i) The total spin S_{tot} of cluster- n is not a good quantum number, while its z -component remains a good quantum number. The ground state of cluster- n has $S_{\text{tot}}^z = 0$ for $D > 0$ and $S_{\text{tot}}^z = \pm 1$ for $D < 0$. Therefore, the $\text{DC}n$ phase with finite n is nonmagnetic for $D > 0$ and paramagnetic for $D \leq 0$.
- (ii) The $\text{DC}\infty$ state corresponds to the ground state of a spin-1 Heisenberg chain that has the single-site anisotropy 0 and D alternatingly. It is known that the ground-state phase diagram of this model consists of a Néel phase for $D \lesssim -0.695$, a Haldane phase for $-0.695 \lesssim D \lesssim 3.28$, and a large- D phase for $D \gtrsim 3.28$.⁴³⁾
- (iii) There appear $\text{DC}n$ phases with $n = 0, 1, 2$, and 3 if λ is above the critical value, which depends on D . These phases continue to the isotropic $\text{DC}n$ phases.

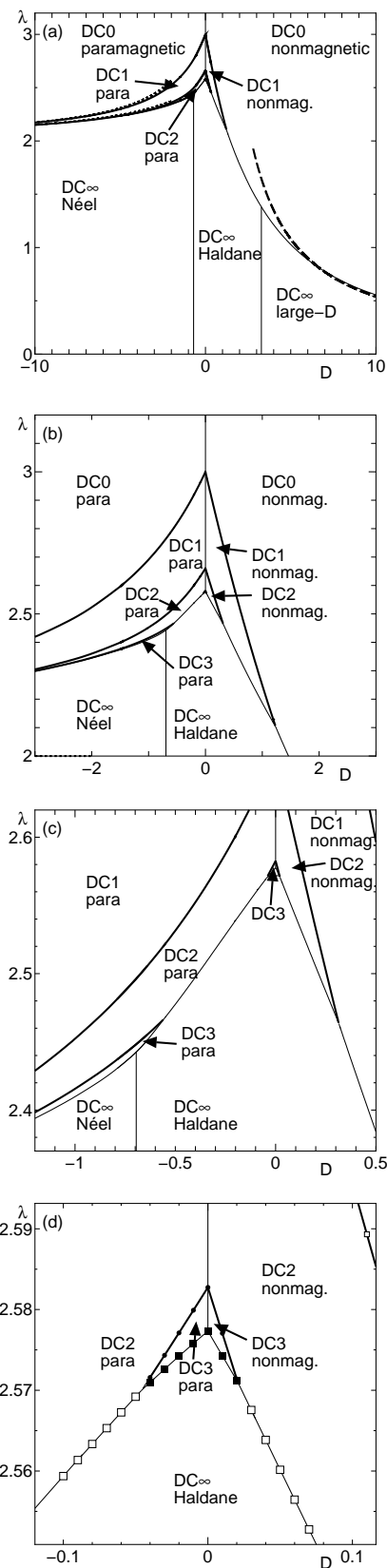


Fig. 2. Ground-state phase diagram of the anisotropic mixed diamond chain. The figures are magnified appropriately from (a) to (d). In (a) and (b), some phases are not indicated because they are invisibly narrow on the scale of these figures. In (a), the analytical results in §3.3 are also shown by the dotted and broken lines.

- (iv) There appears another DC3 phase separated from the line of $D = 0$ and in contact with the end-point of the Néel-Haldane transition line in the $\text{DC}\infty$ region.
- (v) The critical values of λ between the $\text{DC}n$ phases decrease with $|D|$ from those in the isotropic case.
- (vi) For sufficiently large values of $|D|$, only the $\text{DC}0$ and $\text{DC}\infty$ phases exist.

3.3 Limiting cases

3.3.1 $\text{DC}0$ - $\text{DC}1$ phase boundary

The phase boundary between the $\text{DC}0$ and $\text{DC}1$ phases is obtained by substituting the eigenvalues $\tilde{E}_G(1, D)$ and $\tilde{E}_G(3, D)$ into eq. (6). These eigenvalues can be analytically determined. Obviously, $\tilde{E}_G(1, D) = 0$ for $D \geq 0$ and $\tilde{E}_G(1, D) = D$ for $D \leq 0$.

For $D > 0$, the ground state of a cluster- n belongs to the subspace of $S_{\text{tot}}^z = 0$, $P = 1$, and $T = 1$, where S_{tot}^z is the z -component of the total spin, P is the space inversion parity, and T is the time reversal parity. Within this subspace, $\tilde{E}_G(3, D)$ is the smallest solution of the following eigenvalue equation:

$$\begin{aligned} & \tilde{E}_G(3, D)^3 - (3D - 1)\tilde{E}_G(3, D)^2 \\ & + 2(D^2 - D - 3)\tilde{E}_G(3, D) + 8D = 0. \end{aligned} \quad (8)$$

Therefore, $\lambda_c(0, 1) = -\tilde{E}_G(3, D)$. For small values of D , this implies $\lambda_c(0, 1) \simeq 3 - \frac{13}{15}D$.

For $D < 0$, the ground state of a cluster- n belongs to the subspace of $S_{\text{tot}}^z = \pm 1$ and $P = 1$. Within this subspace, $\tilde{E}_G(3, D)$ is the smallest solution of the following eigenvalue equation:

$$\begin{aligned} & \tilde{E}_G(3, D)^4 - (5D - 2)\tilde{E}_G(3, D)^3 \\ & + (8D^2 - 6D - 5)\tilde{E}_G(3, D)^2 \\ & + (-4D^3 + 4D^2 + 14D - 6)\tilde{E}_G(3, D) \\ & - 8D(D - 1) = 0. \end{aligned} \quad (9)$$

Therefore, $\lambda_c(0, 1) = 2D - \tilde{E}_G(3, D)$. For small values of $|D|$, this implies $\lambda_c(0, 1) \simeq 3 + \frac{13}{30}D$.

3.3.2 $D \rightarrow -\infty$

For $D < 0$ and $|D| \gg 1$, we apply the degenerate perturbation theory to the ground-state energy of a cluster- n . We regard the diagonal part of \mathcal{H}_n as the unperturbed Hamiltonian $\mathcal{H}_n^{(0)}$ and the off-diagonal part as the perturbation Hamiltonian $\mathcal{H}_n^{(1)}$ as follows:

$$\begin{aligned} \mathcal{H}_n^{(0)} &= D \sum_{l=1}^{n+1} S_l^{z^2} + \sum_{l=1}^n (S_l^z + S_{l+1}^z) T_l^z, \\ \mathcal{H}_n^{(1)} &= \frac{\alpha}{2} \sum_{l=1}^n [(S_l^+ + S_{l+1}^+) T_l^- + \text{h.c.}]. \end{aligned} \quad (10)$$

The expansion parameter α is introduced, which will be set equal to unity after the calculation. Up to the third-order perturbation calculation in α , we have

$$\tilde{E}_G(2n + 1, D) \simeq - (n + 1)|D| - 2n - \frac{(2n - 2)}{|D| + 3} \alpha^2$$

$$- \frac{2}{|D| + 2} \alpha^2 - \frac{(3n - 3)}{2(|D| + 3)^2} \alpha^3 - \frac{1}{(|D| + 2)^2} \alpha^3 \quad (11)$$

for $n \geq 1$. Substituting this expression into eq. (6), the phase boundaries are determined up to the third order in α as follows.

- (i) The $\text{DC}n$ - $\text{DC}(n + 1)$ transition point for $n \geq 1$ is given by

$$\begin{aligned} \lambda_c(n, n + 1; D) &\simeq 2 + \frac{4}{|D| + 3} \alpha^2 - \frac{2}{|D| + 2} \alpha^2 \\ &+ \frac{3}{(|D| + 3)^2} \alpha^3 - \frac{1}{(|D| + 2)^2} \alpha^3. \end{aligned} \quad (12)$$

The n independence of eq. (12) means the direct transition between the $\text{DC}1$ and $\text{DC}\infty$ phases within this approximation.

- (ii) The $\text{DC}0$ - $\text{DC}1$ transition point is given by

$$\lambda_c(0, 1; D) \simeq 2 \left(1 + \frac{1}{|D| + 2} \alpha^2 + \frac{1}{2(|D| + 2)^2} \alpha^3 \right), \quad (13)$$

where the exact relation $\tilde{E}_G(1, D) = -|D|$ is used.

Setting $\alpha = 1$, these approximate phase boundaries are drawn by the dotted lines in Fig. 2(a).

3.3.3 $D \rightarrow \infty$

In this limit, all the S -spins are in the state $S^z = 0$. Therefore, we find the following:

- (i) The ground-state energy of the $\text{DC}0$ phase is $-\frac{3L}{4}\lambda$.
- (ii) In the $\text{DC}\infty$ phase, the effective interaction between T -spins is $O(1/D)$ as described in ref. 43. The effective Hamiltonian is given by

$$\begin{aligned} \mathcal{H}_{\text{eff}} &= \frac{L}{4} \lambda \\ &+ \sum_{l=1}^L [J_{\text{eff}}(T_l^x T_{l+1}^x + T_l^y T_{l+1}^y) + D_{\text{eff}}(T_l^{z^2} - 2)], \end{aligned} \quad (14)$$

$$J_{\text{eff}} = D_{\text{eff}} = \frac{2}{D}. \quad (15)$$

The ground-state energy of this effective model is calculated by the infinite-size DMRG method as $\frac{\lambda}{4} - 2.6995J_{\text{eff}}$ per site. According to the numerical calculation, there appear no $\text{DC}n$ phases with $1 \leq n < \infty$ for $D > 1.24$. Taking this into account, we conclude that the direct transition between $\text{DC}0$ and $\text{DC}\infty$ phases takes place at

$$\lambda_c(0, \infty; D) \simeq \frac{5.399}{D} \quad (16)$$

for sufficiently large values of D up to $O(1/D)$. This approximate phase boundary is drawn by the broken line in Fig. 2(a).

4. Finite-Temperature Properties

4.1 General formula

Following the method described in ref. 13, we can calculate the thermodynamic expectation value of the extensive quantity Q per unit cell as

$$\frac{\langle Q \rangle}{L} = \frac{\langle Q_{\text{cl}} \rangle}{\langle L_{\text{cl}} \rangle}, \quad (17)$$

where Q_{cl} is the physical quantity Q for each cluster- n and $L_{\text{cl}} \equiv n + 1$ is the number of unit cells per cluster- n . The average $\langle Q_{\text{cl}} \rangle$ of Q_{cl} over the grand canonical ensemble is written as

$$\langle Q_{\text{cl}} \rangle = \frac{\sum_{n=0}^{\infty} Z_{\text{cl}}(n) \langle Q_{\text{cl}}(n) \rangle_{\text{can}} e^{\beta(\mu - \lambda/4)(n+1)}}{\sum_{n=0}^{\infty} Z_{\text{cl}}(n) e^{\beta(\mu - \lambda/4)(n+1)}}, \quad (18)$$

where μ is the chemical potential of a cluster- n . $\langle Q_{\text{cl}}(n) \rangle_{\text{can}}$ and $Z_{\text{cl}}(n)$ are the canonical average of the physical quantity Q and the partition function of a cluster- n with fixed n , respectively. These are defined by

$$\langle Q_{\text{cl}}(n) \rangle_{\text{can}} = \frac{1}{Z_{\text{cl}}(n)} \sum_{M_{\text{cl}}^z} \sum_{\nu} e^{-\beta \tilde{E}(2n+1, \nu; M_{\text{cl}}^z)} \times \langle 2n+1, \nu; M_{\text{cl}}^z | Q_{\text{cl}} | 2n+1, \nu; M_{\text{cl}}^z \rangle, \quad (19)$$

$$Z_{\text{cl}}(n) = \sum_{M_{\text{cl}}^z} \sum_{\nu} e^{-\beta \tilde{E}(2n+1, \nu; M_{\text{cl}}^z)}, \quad (20)$$

where $\tilde{E}(2n+1, \nu; M_{\text{cl}}^z)$ and $|2n+1, \nu; M_{\text{cl}}^z\rangle$ are, respectively, the ν -th eigenenergy and eigenstate of the spin-1 chain with length $2n+1$ and magnetization M_{cl}^z . The chemical potential μ is determined by the condition

$$\sum_{n=0}^{\infty} e^{\beta \lambda} Z_{\text{cl}}(n) e^{\beta(\mu - \lambda/4)(n+1)} = 1. \quad (21)$$

4.2 Formulae for entropy and magnetic susceptibility

The entropy per unit cell is calculated using the same formula as that used in the isotropic case derived in ref. 13 as

$$S = \frac{1}{T} \left(\frac{\langle E_{\text{cl}} \rangle}{\langle L_{\text{cl}} \rangle} - \mu \right). \quad (22)$$

where $E_{\text{cl}} = \tilde{E} + (n-3)\lambda/4$ is the energy per cluster- n .

The longitudinal magnetic susceptibility χ_{\parallel} is calculated using the same formula as that used in the isotropic case by the direct application of eqs. (17), (18), and (20). This gives

$$\chi_{\parallel} = \frac{1}{T} \frac{\langle M_{\text{cl}}^2 \rangle}{\langle L_{\text{cl}} \rangle}. \quad (23)$$

The transverse susceptibility χ_{\perp} is calculated as discussed below.

The contribution to the Hamiltonian due to the transverse field is given by

$$\mathcal{H}_x = -H \sum_{l=1}^L (S_l^x + T_l^x). \quad (24)$$

Because each T_l^2 commutes with \mathcal{H}_x , all T_l 's are conserved even in the presence of the transverse field. Therefore, the magnetic susceptibility of an anisotropic MDC (1) is the sum of the contributions of cluster- n 's.

Using the standard linear response theory, the canonical expectation value of the transverse magnetic susceptibility of a cluster- n is given by

$$\begin{aligned} \langle \chi_{\text{cl}\perp}(n) \rangle_{\text{can}} &= \frac{1}{Z_{\text{cl}}(n)} \sum_{M_{\text{cl}}^z=0}^{2n} \sum_{\nu_1, \nu_2}^{2n} \\ &\times \frac{e^{-\beta \tilde{E}(2n+1, \nu_1; M_{\text{cl}}^z)} - e^{-\beta \tilde{E}(2n+1, \nu_2; M_{\text{cl}}^z+1)}}{\tilde{E}(2n+1, \nu_2; M_{\text{cl}}^z+1) - \tilde{E}(2n+1, \nu_1; M_{\text{cl}}^z)} \\ &\times |\langle 2n+1, \nu_2; M_{\text{cl}}^z+1 | M_{\text{cl}}^+ | 2n+1, \nu_1; M_{\text{cl}}^z \rangle|^2, \end{aligned} \quad (25)$$

where $\tilde{E}(2n+1, \nu; M_{\text{cl}}^z)$ and $|2n+1, \nu; M_{\text{cl}}^z\rangle$ are the ν -th eigenenergy and eigenstate of the spin-1 chain with length $2n+1$ and magnetization M_{cl}^z . Thus, the transverse susceptibility of the MDC per unit cell is given by

$$\chi_{\perp} = \frac{\langle \chi_{\text{cl}\perp} \rangle}{\langle L_{\text{cl}} \rangle}, \quad (26)$$

where $\langle \dots \rangle$ means the grand canonical average defined in eq. (18).

In the DC n ground state, this formula reduces to

$$\begin{aligned} \chi_{\perp} &= \frac{1}{(n+1)} \sum_{\nu} \frac{1}{\tilde{E}(2n+1, \nu; 1) - \tilde{E}_{\text{G}}(2n+1, 0)} \\ &\times |\langle 2n+1, \nu; 1 | M_{\text{cl}}^+ | 2n+1, G; 0 \rangle|^2 \end{aligned} \quad (27)$$

for $D > 0$ and to

$$\begin{aligned} \chi_{\perp} &= \frac{1}{2(n+1)} \sum_{\nu, G} \left[\frac{1}{\tilde{E}(2n+1, \nu; 2) - \tilde{E}_{\text{G}}(2n+1, 1)} \right. \\ &\times |\langle 2n+1, \nu; 2 | M_{\text{cl}}^+ | 2n+1, G; 1 \rangle|^2 \\ &+ \frac{1}{\tilde{E}(2n+1, \nu; 0) - \tilde{E}_{\text{G}}(2n+1, -1)} \\ &\left. \times |\langle 2n+1, \nu; 0 | M_{\text{cl}}^+ | 2n+1, G; -1 \rangle|^2 \right] \end{aligned} \quad (28)$$

for $D < 0$. Here, $|2n+1, G; M_{\text{cl}}\rangle$ is the ground state of a cluster- n with magnetization M_{cl} . For $D < 0$, the ground states are degenerate, so that the summation is taken over all the ground states. It should be noted that χ_{\perp} remains finite at $T = 0$ in both cases.

4.3 Results for entropy and magnetic susceptibility

In eq. (18), the summation over n is taken over all non-negative integers. In the actual numerical calculation of finite-temperature properties, however, we can only include the contribution of cluster- n 's with finite n . Hence, we cannot expect reliable results if the ground state is the DC ∞ state. Therefore, we limit ourselves to the parameter region with DC n ground states with finite n . In what follows, we present the results for the magnetic susceptibility and entropy calculated including the contribution of cluster- n 's with $0 \leq n \leq 5$. The error due to this cutoff procedure is estimated for the isotropic case in ref. 13. Because this estimation is based on an entropic argument in the high-temperature region, it is also valid

in the present case. Thus, we expect that the missing entropy is within 3% of the total entropy.

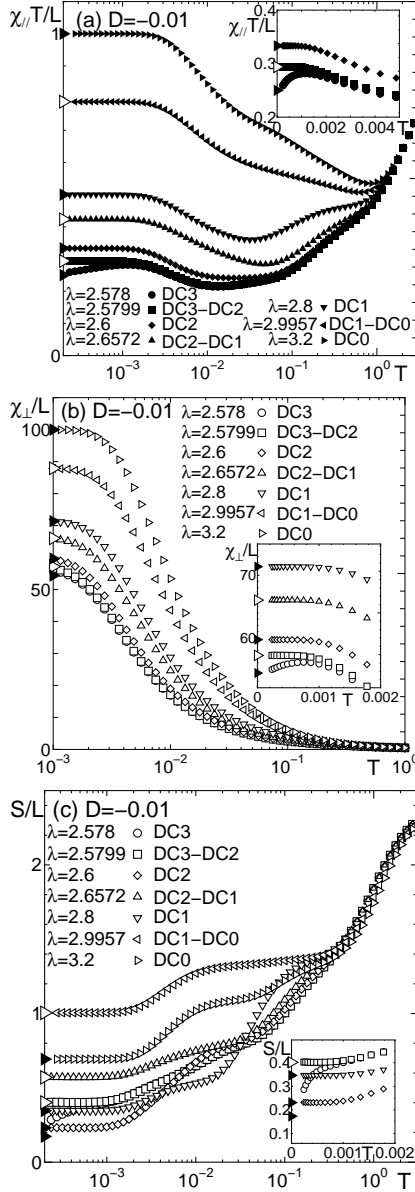


Fig. 3. Temperature dependences of (a) longitudinal magnetic susceptibility $\chi_{||}$ times T , (b) transverse magnetic susceptibility χ_{\perp} , and (c) entropy \mathcal{S} for $D = -0.01$. The chosen values of λ are in the DCn phases and also at the $DC(n+1)$ - DCn phase boundaries. The large filled right triangles on the ordinates are the ground-state values in each phase and the large open ones are those at the phase boundaries. The insets are magnified figures in the low-temperature regimes.

To demonstrate the sensitivity of the low-temperature behavior to the anisotropy D , we present the numerical results for $D = \pm 0.01$ as representatives of the easy-plane and easy-axis anisotropies. For a negative D , the longitudinal and transverse susceptibilities are shown in Figs. 3(a) and 3(b), respectively, and the entropy is shown in Fig. 3(c). For a positive D , both the susceptibilities are shown in Fig. 4(a) and the entropy is shown in Fig. 4(b). The difference between the low-temperature behaviors for the positive and negative D 's is distinct even

for a small $|D| = 0.01$. In the low-temperature limit, the longitudinal magnetic susceptibility $\chi_{||}$ and the entropy \mathcal{S} tend to zero for $D > 0$, except at the ground-state phase boundary. On the other hand, they behave as $\chi_{||}T \simeq \frac{1}{n+1}$ and $\mathcal{S} \simeq \frac{\ln 2}{n+1}$ for $D < 0$ if the ground state belongs to the DCn phase. The low-temperature limiting values of χ_{\perp} are calculated using eqs. (27) and (28). These limiting values are shown by the large filled right triangles on the ordinates in Figs. 3 and 4.

At the $DC(n-1)$ - DCn phase boundary, cluster- $(n-1)$ and cluster- n coexist. In this case, the residual entropy can be estimated by the combinatory argument similarly to that in the isotropic case. If we denote the number fraction of cluster- $(n-1)$'s by x and that of cluster- n 's by $1-x$, then the entropy can be estimated as

$$\mathcal{S} = -\frac{L}{n+1-x} [x \ln x + (1-x) \ln(1-x) - \ln g], \quad (29)$$

where g is the degeneracy of the ground state of cluster- n , i.e., $g = 1$ for $D > 0$, $g = 2$ for $D < 0$, and $g = 3$ for $D = 0$. By optimizing \mathcal{S} with respect to x , we find

$$\frac{x}{g} = \left(\frac{1-x}{x}\right)^n. \quad (30)$$

Using x that satisfies eq. (30), the entropy and susceptibility can be estimated as

$$\frac{\mathcal{S}}{L} = \ln \frac{x}{1-x}, \quad (31)$$

$$\frac{\chi_{||,\perp}}{L} = \frac{x\chi_{cl||,\perp}(n-1) + (1-x)\chi_{cl||,\perp}(n)}{nx + (n+1)(1-x)}. \quad (32)$$

It should be noted that the residual entropy remains finite at the phase boundary even for $D > 0$ owing to the mixing entropy of cluster- $(n-1)$ and cluster- n . For $D < 0$, $\chi_{cl||} = 1/T$ for all n . Therefore, we have

$$\frac{\chi_{||}}{L} = \frac{1}{T(n+1-x)}. \quad (33)$$

For $D > 0$, $\frac{\chi_{||}}{L} = 0$. To calculate χ_{\perp} , we have to estimate $\chi_{cl||,\perp}(n-1)$ and $\chi_{cl||,\perp}(n)$ numerically using eqs. (27) and (28). These low-temperature limiting values are shown by large open right triangles on the ordinates in Figs. 3 and 4.

5. Summary and Discussion

We examined the anisotropic mixed diamond chain with spins 1 and 1/2 that has the single-site anisotropy D on spin-1 sites. In the ground-state phase diagram (Fig. 2), there are DCn phases with $n = 0, 1, 2$, and 3 if λ is above the critical value, which depends on D . These phases continue to the isotropic DCn phases except for a $DC3$ phase separated from the line of $D = 0$. As in the isotropic case, the DCn ground state with finite n is an alternating array of finite-length cluster- n 's and singlet dimers. It is nonmagnetic for the easy-plane anisotropy ($D > 0$), and is paramagnetic for the easy-axis anisotropy ($D < 0$). For smaller λ , the ground-state phase is one of the three $DC\infty$ phases: i.e., the Néel phase for

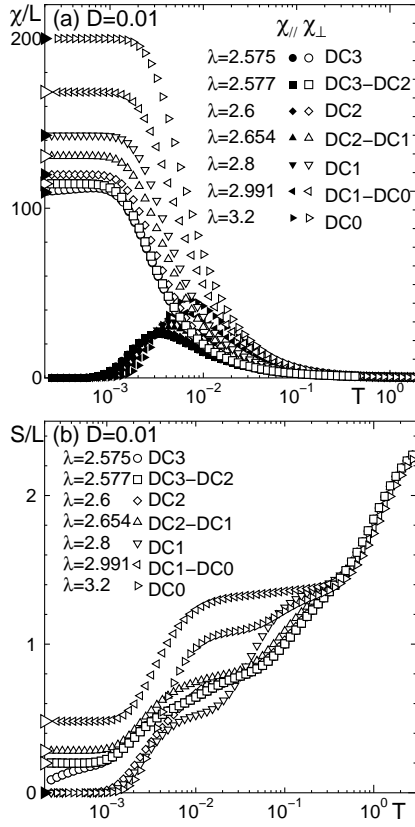


Fig. 4. Temperature dependences of (a) longitudinal (χ_{\parallel}) and transverse (χ_{\perp}) magnetic susceptibilities and (b) entropy S for $D = 0.01$. The chosen values of λ are in the DC n phases and also at DC($n+1$)-DC n phase boundaries. The large filled right triangles on the ordinates are the ground-state values in each phase and the large open ones are those at the phase boundaries.

$D \lesssim -0.695$, the Haldane phase for $-0.695 \lesssim D \lesssim 3.28$, and the large- D phase for $D \gtrsim 3.28$. The critical values of λ between the DC n phases decrease with $|D|$ from those in the isotropic case. For sufficiently large values of $|D|$, only the DC0 and DC ∞ phases exist. The phase boundary between them tends to $\lambda=2$ for $D \rightarrow -\infty$ and to $\lambda=0$ for $D \rightarrow \infty$.

The above features of the ground-state phase diagram are qualitatively understood, if we incorporate the effect of quantum fluctuation into the classical phase diagram explained in Appendix. In the two classical phases with $\lambda > 2$, a pair of $\tau_i^{(1)}$ and $\tau_i^{(2)}$ can locally rotate around the fixed axis determined by S_i 's without increasing the energy, as seen in Appendix. The anisotropic term restricts the possible direction of the fixed axis: for $D < 0$, the fixed axis is only parallel or antiparallel to the z -axis, and for $D > 0$ it is confined in the xy plane. The quantum effect of D corresponding to this classical restriction is to reduce the quantum fluctuation of S_i 's only. Therefore, for $\lambda \gtrsim 2$, the anisotropic term does not suppress the quantum fluctuation corresponding to the classical local rotations of $\tau_i^{(\nu)}$'s around the fixed axis of S_i . On the other hand, for $\lambda \lesssim 2$, the classical ground state is antiferromagnetically ordered so that the quantum fluctuation is collectively concerned with all the spins and is not restricted to individual pairs of $\tau_i^{(1)}$ and $\tau_i^{(2)}$. There-

fore, the D -term suppresses the collective quantum fluctuation, and hinders the energy gain by the quantum fluctuation. This explains the reason why the region of the exotic ground state for large λ extends to lower values of λ with an increase in the magnitude of the anisotropy $|D|$.

The features of the ground-state phases and phase transitions are reflected in physical quantities at low temperatures. The temperature dependences of entropy, and longitudinal and transverse susceptibilities are calculated. The low-temperature behavior is sensitive to the sign of D for large λ , reflecting the change of the ground-state phase. The transverse susceptibility remains finite even at $T = 0$, as long as $D \neq 0$.

Generally, the introduction of anisotropy to a physical model increases the possibility that a corresponding material is realized. If an anisotropic MDC material is synthesized, the anisotropy may be controlled by changing the crystal field that reflects the environment of spin-1 magnetic ions. This would be accomplished by, e.g., applying pressure and/or changing the nonmagnetic ions around the magnetic ones. In contrast to the spin-1 chain with the Haldane gap, the ground state of the MDC is sensitive to the weak anisotropy. Therefore, the paramagnetic-nonmagnetic transition should take place with a small variation in the crystal field. It would also be possible to observe the quantum phase transitions between the DC n states with different spatial periodicities.

In refs. 14 and 15, we have reported the effect of distortion on the isotropic MDC. It is predicted that various types of distortion can induce various types of quantum phases such as the Haldane phase with STSB, and the quantized and partial ferrimagnetic phases. The interplay of anisotropy and distortion would lead to an even wider variety of phenomena. Their investigation is left for future studies.

The numerical diagonalization program is based on the package TITPACK ver.2 coded by H. Nishimori. The numerical computation in this work has been carried out using the facilities of the Supercomputer Center, Institute for Solid State Physics, University of Tokyo, the Supercomputing Division, Information Technology Center, University of Tokyo, and the Yukawa Institute Computer Facility, Kyoto University. KH is supported by a Grant-in-Aid for Scientific Research (C) (21540379) from the Japan Society for the Promotion of Science.

Appendix

We examine the phase diagram of the classical version of the quantum Hamiltonian (2), where S_i and $\tau_i^{(\nu)}$ are interpreted as classical vectors with length S and $\tau = S/2$, respectively. The classical Hamiltonian is then expressed in the following two forms:

$$\mathcal{H}^{\text{clas}} = \frac{1}{4} \sum_l \left[(2T_l + \hat{S}_l)^2 - 2(2-\lambda)T_l^2 - \hat{S}_l^2 \right] + \mathcal{H}_1^{\text{clas}} \quad (34)$$

$$= \frac{1}{4\lambda} \sum_l \left[2(\lambda T_l + \hat{S}_l)^2 - 2\hat{S}_l^2 \right] + \mathcal{H}_1^{\text{clas}}, \quad (35)$$

where $\hat{\mathbf{S}}_l \equiv \mathbf{S}_l + \mathbf{S}_{l+1}$, $\mathbf{T}_l \equiv \boldsymbol{\tau}_l^{(1)} + \boldsymbol{\tau}_l^{(2)}$, and $\mathcal{H}_1^{\text{clas}} \equiv \sum_{l=1}^L (DS_l^z - \lambda S^2/4)$.

In the case of $\lambda \leq 2$, the expression (34) shows that $\mathcal{H}^{\text{clas}}$ is minimized if $|\hat{\mathbf{S}}_l| = 2S$, $|\mathbf{T}_l| = S$, and $|\mathbf{T}_l + \frac{1}{2}\hat{\mathbf{S}}_l| = 0$ irrespective of D . Hence, all the \mathbf{S}_l 's ($\boldsymbol{\tau}_l^{(\alpha)}$'s) in the chain are aligned parallel (antiparallel) to a fixed axis, and the ground state is antiferromagnetic. The fixed axis is the z -axis for $D < 0$, while it may be any direction in the xy plane for $D > 0$. The ground state is elastic in both cases, since any local modification of the spin configuration increases the energy.

In the case of $\lambda > 2$, the expression (35) reveals that $\mathcal{H}^{\text{clas}}$ is minimized if $|\hat{\mathbf{S}}_l| = 2S$ and $|\mathbf{T}_l + \hat{\mathbf{S}}_l/\lambda| = 0$ irrespective of D . Hence, \mathbf{S}_l 's in the chain are aligned parallel to a fixed axis, and $\boldsymbol{\tau}_l^{(1)}$ and $\boldsymbol{\tau}_l^{(2)}$ form a triangle with $\hat{\mathbf{S}}_l/\lambda$. The fixed axis is the z -axis for $D < 0$, while it may be any direction in the xy plane for $D > 0$. Then, the ground state has a local arbitrariness, because $\boldsymbol{\tau}_l^{(1)}$ and $\boldsymbol{\tau}_l^{(2)}$ may be rotated about the axis of \mathbf{S}_l and \mathbf{S}_{l+1} without raising the energy. All the ground states are ferrimagnetic with a magnetization $(1 - 2/\lambda)SN$.

Thus, we have the classical phase diagram consisting of the four phases separated by the phase boundaries of $\lambda = 2$ and $D = 0$.

- 1) *Frustrated Spin Systems*, ed. H. T. Diep: (World Scientific, Singapore, 2005) Chaps. 5 and 6.
- 2) *Introduction to Frustrated Magnetism: Materials, Experiments, Theory*, ed. C. Lacroix, P. Mendels, and F. Mila: (Springer Series in Solid-State Sciences, Springer, Heidelberg, 2011).
- 3) C. K. Majumdar and D. K. Ghosh: *J. Math. Phys.* **10** (1969) 1399.
- 4) For examples of experimental materials, see M. Hase, H. Kuroe, K. Ozawa, O. Suzuki, H. Kitazawa, G. Kido, and T. Sekine: *Phys. Rev. B* **70** (2004) 104426.
- 5) B. S. Shastry and B. Sutherland: *Physica B+C* **108** (1981) 1069.
- 6) H. Kageyama, K. Yoshimura, R. Stern, N.V. Mushnikov, K. Onizuka, M. Kato, K. Kosuge, C.P. Slichter, T. Goto, and Y. Ueda: *Phys. Rev. Lett.* **82** (1999) 3168.
- 7) H. Kageyama, M. Nishi, N. Aso, K. Onizuka, T. Yoshizawa, K. Nukui, K. Kodama, K. Kakurai, and Y. Ueda: *Phys. Rev. Lett.* **84** (2000) 5876.
- 8) K. Takano: *J. Phys. A: Math. Gen.* **27** (1994) L269.
- 9) K. Takano, K. Kubo, and H. Sakamoto: *J. Phys. Condens. Matter* **8** (1996) 6405.
- 10) H. Niggemann, G. Uimin, and J. Zittartz: *J. Phys. Condens. Matter* **9** (1997) 9031.
- 11) H. Niggemann, G. Uimin, and J. Zittartz: *J. Phys. Condens. Matter* **10** (1998) 5217.
- 12) K. Takano, H. Suzuki, and K. Hida: *Phys. Rev. B* **80** (2009) 104410.
- 13) K. Hida, K. Takano, and H. Suzuki: *J. Phys. Soc. Jpn.* **78** (2009) 084716.
- 14) K. Hida, K. Takano, and H. Suzuki: *J. Phys. Soc. Jpn.* **79** (2010) 044702.
- 15) K. Hida, K. Takano, and H. Suzuki: *J. Phys. Soc. Jpn.* **79** (2010) 114703.
- 16) K. Okamoto, T. Tonegawa, Y. Takahashi, and M. Kaburagi: *J. Phys. Condens. Matter* **11** (1999) 10485.
- 17) K. Okamoto, T. Tonegawa, and M. Kaburagi: *J. Phys. Condens. Matter* **15** (2003) 5979.
- 18) K. Sano and K. Takano: *J. Phys. Soc. Jpn.* **69** (2000) 2710.
- 19) N. B. Ivanov, J. Richter, and J. Schulenburg: *Phys. Rev. B* **79** (2009) 104412.
- 20) H. Kikuchi, Y. Fujii, M. Chiba, S. Mitsudo, T. Idehara, T. Tonegawa, K. Okamoto, T. Sakai, T. Kuwai, and H. Ohta: *Phys. Rev. Lett.* **94** (2005) 227201.
- 21) H. Ohta, S. Okubo, T. Kamikawa, T. Kunimoto, Y. Inagaki, H. Kikuchi, T. Saito, M. Azuma, and M. Takano: *J. Phys. Soc. Jpn.* **72** (2003) 2464.
- 22) A. Izuoka, M. Fukada, R. Kumai, M. Itakura, S. Hikami, and T. Sugawara: *J. Am. Chem. Soc.* **116** (1994) 2609.
- 23) D. Uematsu and M. Sato: *J. Phys. Soc. Jpn.* **76** (2007) 084712.
- 24) N.B. Ivanov and J. Richter: *Phys. Lett. A* **232** (1997) 308.
- 25) J. Richter, N. B. Ivanov, and J. Schulenburg: *J. Phys. Condens. Matter* **10** (1998) 3635.
- 26) A. Koga, K. Okunishi, and N. Kawakami: *Phys. Rev. B* **62** (2000) 5558.
- 27) A. Koga and N. Kawakami: *Phys. Rev. B* **65** (2002) 214415.
- 28) J. Schulenburg and J. Richter: *Phys. Rev. B* **65** (2002) 054420.
- 29) J. Schulenburg and J. Richter: *Phys. Rev. B* **66** (2002) 134419.
- 30) T. Hakobyan, J. H. Hetherington, and M. Roger: *Phys. Rev. B* **63** (2001) 144433.
- 31) L. Čanová, J. Strečka, and M. Jasčúr: *J. Phys. Condens. Matter* **18** (2006) 4967.
- 32) L. Čanová, J. Strečka, and T. Lučivjanský: *Condens. Matter Phys.* **12** (2009) 353.
- 33) H. Kobayashi, Y. Fukumoto, and A. Oguchi: *J. Phys. Soc. Jpn.* **78** (2009) 074004.
- 34) H. J. Schulz: *Phys. Rev. B* **34** (1986) 6372.
- 35) M. den Nijs and K. Rommels: *Phys. Rev. B* **40** (1989) 4709.
- 36) H. Tasaki: *Phys. Rev. Lett.* **66** (1991) 798.
- 37) T. Kennedy and H. Tasaki: *Phys. Rev. B* **45** (1992) 304.
- 38) W. Chen, K. Hida, and B. C. Sanctuary: *Phys. Rev. B* **67** (2003) 104401.
- 39) M. Oshikawa: *J. Phys. Condens. Matter* **4** (1992) 7469.
- 40) T. Tonegawa, K. Okamoto, H. Nakano, T. Sakai, K. Nomura, and M. Kaburagi: *J. Phys. Soc. Jpn.* **80** (2011) 043001.
- 41) T. Tonegawa, K. Okamoto, T. Sakai, and M. Kaburagi: *J. Phys. Conf. Ser.* **145** (2009) 012066.
- 42) T. Tonegawa, T. Sakai, K. Okamoto, and M. Kaburagi: *J. Phys. Soc. Jpn.* **76** (2007) 124701.
- 43) K. Hida and W. Chen: *J. Phys. Soc. Jpn.* **74** (2005) 2090.
- 44) K. Hida: *J. Phys. Soc. Jpn.* **76**, 024714 (2007).
- 45) See for example *Magnetism: Molecules to Materials I-V*, ed. J. S. Miller and M. Drillon: (Wiley, Weinheim, 2001-2005).